LAWRENCE
LIVERMORE
NATIONAL
LABORATORY

LLNL-JRNL-610433

Fatigue cracking of a bare steel first wall in an inertial fusion chamber

R. M. Hunt, R. P. Abbott, M. A. Havstad, A. M. Dunne

January 15, 2013

Fusion Engineering and Design

Disclaimer

This document was prepared as an account of work sponsored by an agency of the United States government. Neither the United States government nor Lawrence Livermore National Security, LLC, nor any of their employees makes any warranty, expressed or implied, or assumes any legal liability or responsibility for the accuracy, completeness, or usefulness of any information, apparatus, product, or process disclosed, or represents that its use would not infringe privately owned rights. Reference herein to any specific commercial product, process, or service by trade name, trademark, manufacturer, or otherwise does not necessarily constitute or imply its endorsement, recommendation, or favoring by the United States government or Lawrence Livermore National Security, LLC. The views and opinions of authors expressed herein do not necessarily state or reflect those of the United States government or Lawrence Livermore National Security, LLC, and shall not be used for advertising or product endorsement purposes.

Fatigue cracking of a bare steel first wall in an inertial fusion chamber

R.M. Hunt[a,*], R.P. Abbott[a], M.A. Havstad[a], A.M. Dunne[a]

[a]*Lawrence Livermore National Laboratory, 7000 East Ave, Livermore, CA, 94550, USA*

Abstract

Inertial confinement fusion power plants will deposit high energy X-rays onto the outer surfaces of the first wall many times a second for the lifetime of the plant. These X-rays create brief temperature spikes in the first few microns of the wall, which cause an associated highly compressive stress response on the surface of the material. The periodicity of this stress pulse is a concern due to the possibility of fatigue cracking of the wall. We've used finite element analyses to simulate the conditions present on the first wall in order to evaluate the driving force of crack propagation on fusion-facing surface cracks.

Analysis results indicate that the X-ray induced plastic compressive stress creates a region of residual tension on the surface between pulses. This tension film will likely result in surface cracking upon repeated cycling. Additionally, the compressive pulse may induce plasticity ahead of the crack tip, leaving residual tension in its wake. However, the stress amplitude decreases dramatically for depths greater than $80 - 100\ \mu$m into the fusion-facing surface. Crack propagation models as well as strain-life estimates agree that even though small cracks may form on the surface of the wall, they are unlikely to propagate further than $100\ \mu$m.

Keywords: first wall, fatigue, thermomechanical stress, crack propagation

1. Introduction

In an inertial confinement fusion (ICF) chamber, each fusion shot releases high-energy X-rays and 14 MeV neutrons which are captured and converted to thermal energy in the fusion blanket. While the neutrons penetrate deep into the blanket, the X-rays are absorbed in the outer few microns of the first wall. These X-rays have an intensity and breadth that is dependent on the gas pressure inside the chamber. Increased gas pressure absorbs the highest energy X-rays and re-radiates the energy over a time scale long enough to avoid melting a solid first wall. Still, the reaction produces a temperature spike and a related compressive stress spike on the outer surface due to thermal expansion of the material. The compressive stress spike is a potential concern for the survival of the first wall because the X-ray loading is a cyclic process and may induce fatigue cracking over the lifetime of the component.

Though a variety of materials are being considered as candidates for the first wall in ICF chambers, reduced-activation ferritic martensitic (RAFM) steels are particularly attractive, in part for their material properties under high irradiation doses. Among RAFM steels, grades with 12% chromium content have shown superior ductile-to-brittle transition temperature properties when irradiated in temperature ranges that are applicable to ICF systems [1]. One such 12Cr steel is Sandvik HT-9, which is used in this study as an example ferritic martensitic steel that may resemble the finally selected material. Actual selection of the first wall material will be contingent on further research.

A compressive applied cyclic load, though often ignored in fatigue analysis, can still cause crack initiation and growth [2, 3]. To this effect, a single sharp compressive load can create a plastic zone near the tip of the crack, which, when removed, will result in residual tensile stress in the wake of the plasticity [3]. Tension at the crack tip causes the crack to grow at a decreasing rate until it arrests [2, 3]. Critical to the survival of the first wall is therefore a thorough understanding of the relationship between the cyclic stress field and crack propagation.

Though it can give a simple estimate of cycle lifetime, the standard stress-life approach to fatigue analysis fails to capture more detailed effects associated with the intense compressive loads of the first wall. Specifically, in cases where the maximum compression is large relative the minimum, (e.g. $R < -1$), the correct R ratio should be used to establish lifetime predictions. However, crack propagation measurements at compressive R ratios are seldom performed because commonly used test specimen are designed only for tensile loading [4].

To compliment stress-based fatigue analysis, the crack-growth method assumes three regimes for crack propagation [4]. When the stress intensity factor exceeds the plane strain fracture toughness of the material, K_{IC}, the crack will propagate under fast fracture. Under stable crack growth, cracks will grow as a function of the applied stress intensity factor range, ΔK, and stress ratio, R.

$$\frac{da}{dN} = f(\Delta K, R)$$

where a is the crack size, N is the number of loading cycles.

*Corresponding author. Tel.: 310.893.9117; fax: 925.422.5934

Email addresses: hunt52@llnl.gov (R.M. Hunt), abbott13@llnl.gov (R.P. Abbott), havstad1@llnl.gov (M.A. Havstad), dunne8@llnl.gov (A.M. Dunne)

As ΔK decreases, so too does the crack growth rate. When the stress intensity factor range produces a crack growth rate below 10^{-7} mm/cycle, the growth rate is generally considered negligible. This point is called the threshold stress intensity range, ΔK_{th}. For HT-9 steel in air at room temperature, ΔK_{th} has been measured to be 6.8 MPa $\sqrt{\text{m}}$, much less than the material's plane strain fracture toughness, which is on the order of 100 MPa $\sqrt{\text{m}}$ [5]. However, assuming a repetition rate of 8 Hz for at least a year of fusion operation, an ICF system will need to survive at least 250 million cycles. With such a long design lifetime on a relatively thin wall, even this rate of crack growth may be unacceptable. Obtaining accurate material data is therefore paramount to safe component design in ICF systems.

2. Approach

To assess whether operational fusion loads can lead to fracture through the thickness of the first wall, we have simulated the X-ray transient pulses using a two-dimensional ANSYS thermal-mechanical model. This 2D model calculated temperature and stress response with respect to time on a cross-section segment of a first wall tube or panel (see Fig. 1).

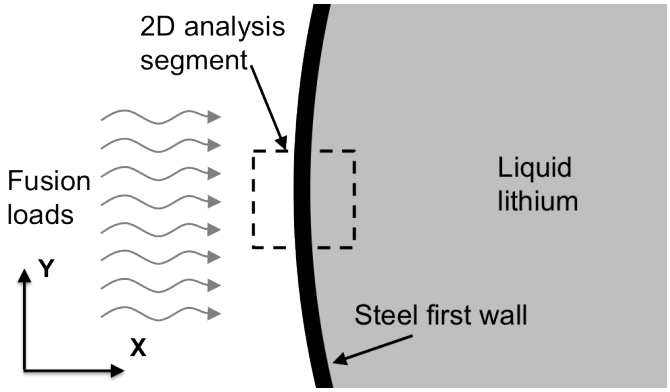

Figure 1: The two-dimensional model simulates operational loads on a cross-section of a thin first wall geometry.

The ANSYS model was designed as a fully transient thermal model that is sequentially coupled to a quasi-static structural model. The static structural model solves at discrete time intervals, based on temperature loads read from the transient thermal model.[1] To achieve good resolution of the 1 ms X-ray pulse, time stepping was heavily biased towards the start of each pulse, with longer time steps between shots.

The two-dimensional model was configured in the plane-strain condition (zero strain in the out-of-plane direction). To confirm the accuracy of both the spacial and temporal accuracy of the simple 2D model, a fully-transient, three-dimensional model was created using TOPAZ3D/DYNA. This model used a coarser mesh by comparison, but modeled an entire tube geometry (see Fig. 2).

[1] This method does not account for inertial terms in the static solution, so the structural solution make be slightly over-estimated. However, these effects should be marginal; within 160 ns a deformation wave can propagate through the thickness of the wall.

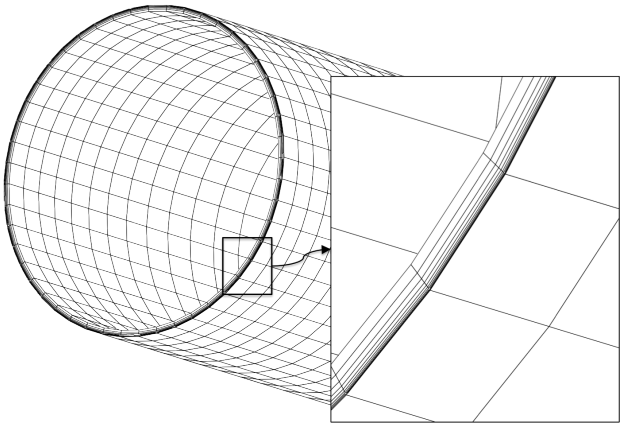

Figure 2: Three-dimensional mesh of a first wall tube for analysis in TOPAZ3D/DYNA

A proposed ICF first wall design relies on very thin steel tubes to carry liquid lithium as a heat transfer medium. The slimness of the steel allows the lithium coolant to maintain a low average temperature gradient in the structural steel. We calculated the temperature in the wall based on a simplified square, 1 ms wide X-ray pulse. The X-ray pulse in this calculation equates to a surface heat flux of 66.6 MW/m^2, which is based on the assumption that X-ray output will be 22% of a 1,096 MW fusion power system in a 6 m radius chamber.

$$P_{xray} = 0.22 P_{fusion} = 241 \text{ MW}$$

$$q''_{ave} = \frac{P_{xray}}{4\pi R^2} = 0.53 \text{ MW/m}^2$$

$$q''_{pulse} = \frac{q''}{\tau f} = 66.6 \text{ MW/m}^2$$

where the X-rays are modeled as a square pulse, with τ = 1 ms width and f = 8 Hz frequency. For this calculation, we have assumed a 1 mm thick section of HT-9 (see Appendix for HT-9 material properties). We also assumed a steady state convection criteria of liquid lithium with a heat transfer coefficient of 20 kW/m^{2}K and a bulk temperature of 743 K (470 °C).

For the structural simulation, we've used cyclic stress-strain data to simulate the response of the region after plastic shakedown. Using monotonic material properties would give a significantly higher alternating stress amplitude at the front surface, but would incorrectly distribute strain in the cyclic regime.

Since the first wall steel will be operating at elevated temperatures, failure under fatigue is likely to occur via ductile fracture rather than brittle fracture. To capture the elastic-plastic fracture, we used the J-integral method, which calculates the energy release rate of crack propagation using a path-independent integral [6].

$$J = \int_\Gamma \left(W n_1 - t_i \frac{\partial u_i}{\partial x_1} \right) d\Gamma$$

where u is displacement, t is the traction vector, W is the strain-energy density, and n is the unit normal. Because the integral is path-independent, the calculation can be made relatively far

away from the crack tip in order to nullify the erroneous stress magnitudes reported at the crack tip singularity [7]. The resulting J value can be compared to the material's ductile fracture toughness, J_{IC}, or converted to the brittle fracture toughness, K_{IC} to quantify crack propagation using the following equation:

$$K_I = \sqrt{JE'}$$

where E' is equal to $E/(1-\nu^2)$ for plane strain, and is equal to E for plane stress [6]. Rather than attempt to model a growing crack in ANSYS, we calculated the maximum stress intensity factor for two-dimensional first wall models with static crack lengths of 15 μm, 25 μm, 50 μm, 75 μm, 100 μm, and 200 μm. These data were sufficient to create a trend in the stress intensity factor with respect to crack length.

At the crack tip, the 8-node planar elements used throughout the model have been collapsed into triangles with three nodes at the crack tip. These elements capture the stress singularity condition present at any finite element analysis at a sharp corner. Using these elements confines the singularity to a single row of elements, which improves stress accuracy in the neighboring rows. Only half of the crack was modeled, as the model contains a horizontal symmetry condition along the crack plane (see Fig. 3). Contact elements span the crack face to prevent the crack face from extended past its symmetric pair. This method is based on the model developed by Blanchard for a tungsten armored first wall [8].

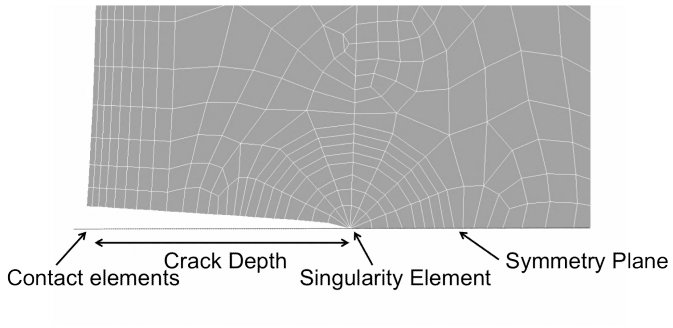

Figure 3: A simple 2D geometry measured stress intensity of a crack under thermal loading. The crack propagation model in ANSYS included contact elements along the crack face to allow opening and closing of the crack.

3. Findings

The thermally-induced compressive spike creates residual tensile stresses near the outer surface of the steel first wall, which can drive surface crack propagation. The first process by which this occurs is via residual surface tension left in the wake of plastic compression. The second process is from the reversed stress region (also a residual stress) that appears ahead of an open crack tip during cyclic loading. These two effects result in stress intensity values only slightly below the material's threshold crack propagation limit. However, the stress intensity decays as cracks grow into the material (resulting in crack arrest), due to the fall-off of thermal-stress away from the fusion-facing surface. This section discusses the results from the thermal-mechanical analysis, reviews the likelihood of failure using the stress-life estimate, and lastly evaluates crack propagation using the J-integral method.

3.1. Thermal-mechanical quasi-static response

Based on the loads described in the previous section, the surface temperature of a 1 mm thick first wall is expected to exceed 900 K after every fusion shot (Fig. 4). This X-ray induced thermal pulse creates a large compressive stress that initially extends only a few microns into the wall. This spike moves through the material with the speed of the traveling thermal wave, decaying as it travels.

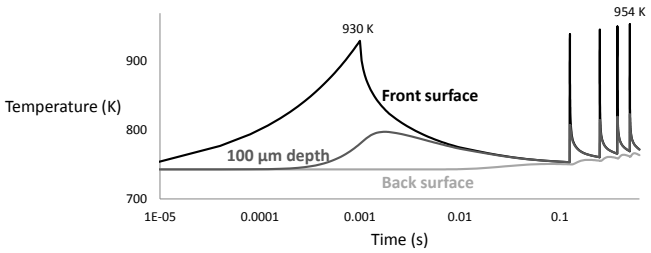

Figure 4: The first walls will receive brief, high-temperature pulses on the fusion-facing surfaces, resulting in temperatures in excess of 900 K.

Ignoring for a moment the plasticity of steel and modeling the first wall instead as a purely elastic material, the compressive spike exceeds 600 MPa in the crack normal direction (Fig. 5a). Behind this compressive spike, the rest of the wall goes slightly into tension to equilibrate the stress distribution through the volume.

Including plasticity complicates the model slightly. Instead of the sharp compressive stress spike, yielding limits the stress at 246 MPa, and the energy is absorbed in the plastic straining of the material (see Fig. 5b). The energy from a 1 ms X-ray pulse is sufficient to plasticize a depth of less than 100 μm. During cooling, this plastic film is pulled into tension by the elastic response of the rest of the wall. This elastic response is actually strong enough to create plastic tension in a small thickness of the wall closest to the surface. A hysteresis plot (see Fig. 6) shows this process clearly; the front face is pulled back to a near-zero strain, to match the elastic nature of the bulk wall. This region of plasticity is not at much risk to ratcheting since the plastic layer is so thin and will not soften any more than the cyclic stress-strain data used for this calculation. Beyond the plastic region, the material cycles in compression only (see "100 μm depth" curve in Fig. 5b).

Using TOPAZ3D/DYNA, a fully-transient, 3D model showed hoop stresses at $\theta = 0°$ (facing the fusion chamber center) that closely resembled the normal stresses in the 2D ANSYS calculations. The magnitude of the stress spike falls off significantly with increasing θ and is non-existent by $\theta = 45°$. The back side of the tube appears to vibrate in response to the stress spike at very high frequency (see Fig. 7).

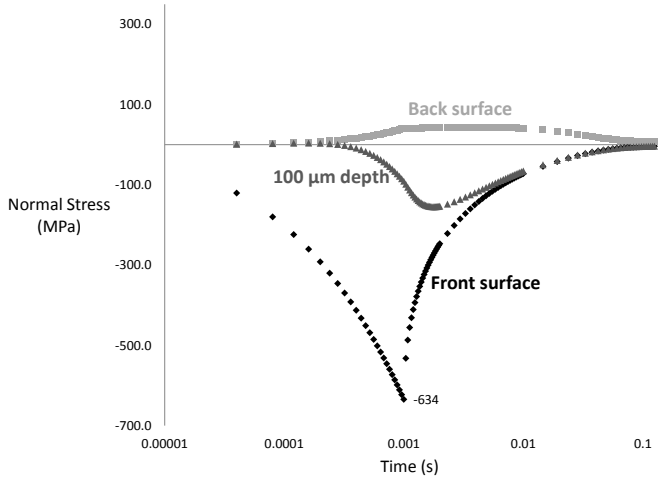

(a) Elastic Model

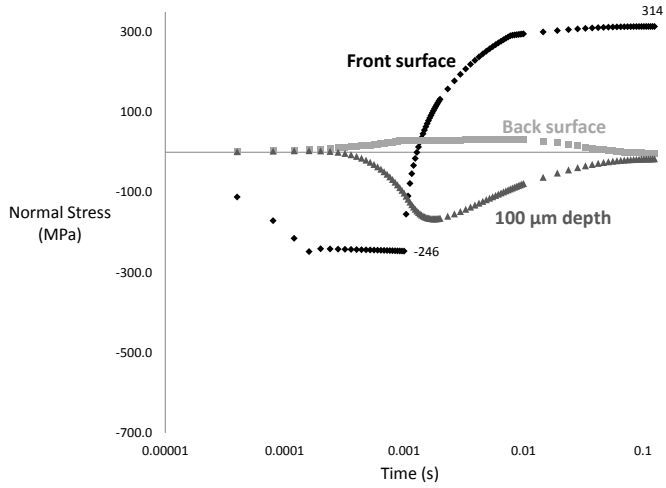

(b) Plastic Model

Figure 5: The high-temperature pulses create corresponding compressive stress spikes near the surface of the wall. When plasticity is included, the stress spike reaches yield point at 246 MPa near the surface of the wall, and then is pulled into tension prior to the next pulse.

Beyond the plastic surface film, the wall springs back only until it reaches a neutral stress state. However, residual tension can also be present at crack tips, irregardless of the plastic zone thickness. If cracks have some initial opening depth then the compressive pulse will drive the crack closed, creating a compressive plastic zone near the crack tip. When the thermal pulse relaxes and the crack opens, residual tensile stress is produced at the crack tip.

The tensile region surrounding the crack tip can propagate the crack to the extent of the "cyclic" plastic stress region, which should have a radius smaller than the monotonic plastic region, as follows:

$$2r'_{0\sigma} \approx \frac{1}{\pi}\left[\frac{\Delta K}{2\sigma_0}\right]^2$$

where σ_0 is the applied compressive stress [9].

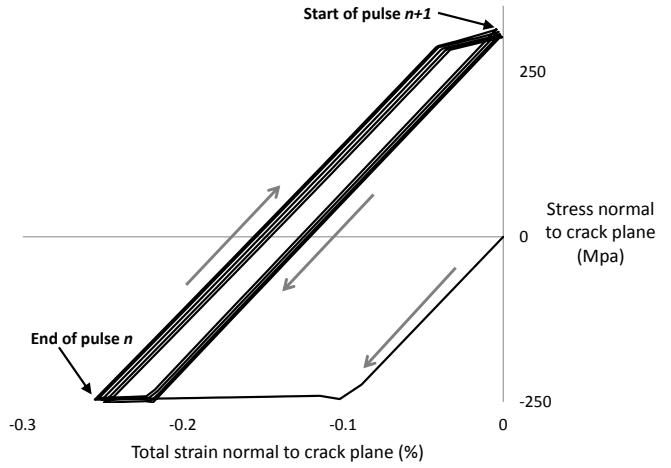

Figure 6: Hysteresis plot at the surface of the wall. The first pulse drives the surface into plastic compression. The ensuing elastic spring-back of the bulk of the wall pulls the plasticized region into tension.

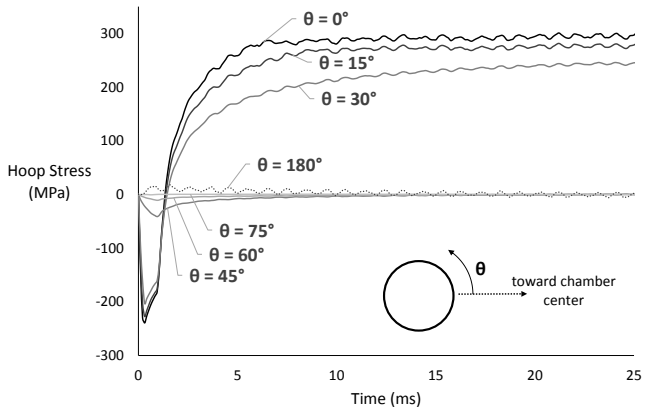

Figure 7: The 3D tube geometry modeled in TOPAZ3D/DYNA reveals that the transient stress spike occurs only in a 90° wedge facing the fusion chamber center. The magnitude of the peak stress when $\theta = 0$ agrees with 4% of the 2D plane-strain model.

The behavior predicted by the finite element analysis matches well with the theory. Between thermal pulses, there is a region of tensile stress (the reversed "cyclic" region) immediately ahead of the crack tip (as seen in Fig. 8). Though the magnitude of the stress is distorted by the numerical singularity of the crack tip, the shape of this tensile area matches well with the shape of plasticity expected from fracture mechanics theory. The crack sees a tensile driving force that could cause propagation even after the crack has left the plastic surface film. However, this tensile stress region shrinks as the crack grows into the wall, indicating crack arrest (Fig. 8). Evaluating the location of crack arrest is hindered by the stress singularity, and must therefore be addressed using J-integral, which takes this singularity into account.

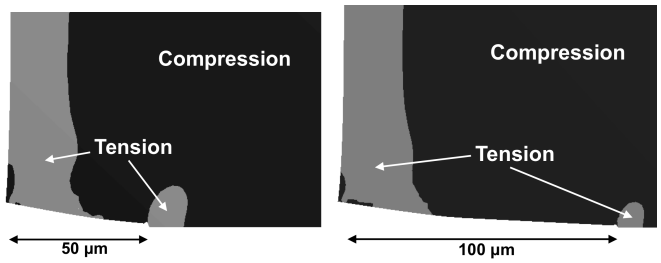

(a) 50 μm crack (b) 100 μm crack

Figure 8: Cracks modeled with an initial opening width contain a reversed tensile stress region near the crack tip during relaxation between pulses. As the crack extends, the tensile region around the crack tip (the driving force of propagation) decreases.

3.2. Fatigue failure assessment

To predict fatigue lifetime, the complex stress-space-time profiles must first be simplified into alternating and mean stresses and strains. These values are calculated from the extremums of the stress at every spatial point through of the wall. One of these extremums occurs at the same time in the entire wall: at the very end of each cycle, just before the ensuing X-ray pulse. However, the other extremum occurs based on the thermal wave propagating through the wall, and is therefore dependent on the distance from the fusion-facing surface (i.e. the peak stress at a point just beneath the surface occurs a few micro-seconds after the peak stress on the surface). To capture this extremum is a matter of plotting the maximum and minimum stresses through the wall at every point in time (see Fig. 9).

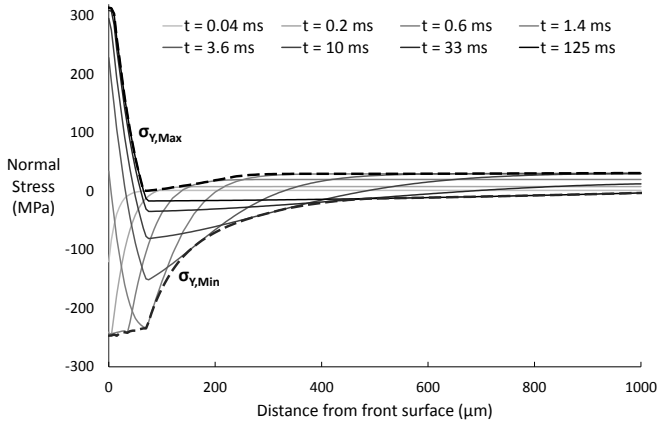

Figure 9: Hoop stress through the thickness of the wall (on a plane far from the crack plane) for multiple points in time. The combination of all points in time gives the shape of the maximum and minimum stress values for fatigue calculation.

While high-cycle, elevated-temperature fatigue data is not currently available for HT-9, there are data for low-cycle fatigue for EUROFER97 at 500 °C [10]. To obtain information on high-cycle fatigue for a RAFM material, we have extrapolated the EUROFER97 data to beyond 250 million cycles (Fig. 10). To account for the crudeness of this approximation, we implemented a safety factor of 2 on strain range for actual calculation of fatigue life. For the material to last 250 million cycles, the design curve predicts a critical strain range of 0.08%.

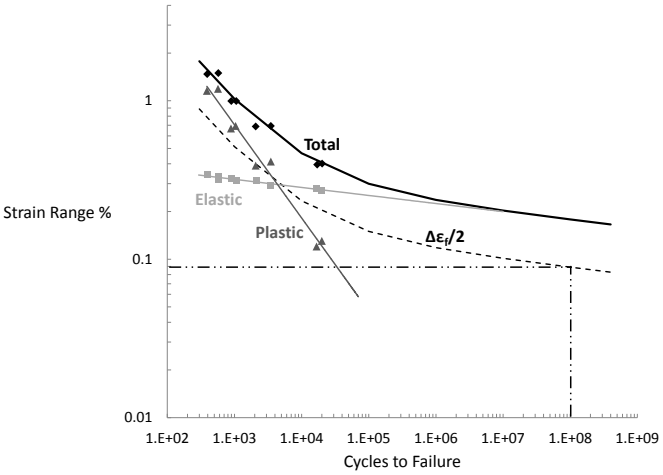

Figure 10: Extrapolating the low cycle fatigue data of EUROFER97 at 500 °C gives a very crude estimate of the strain amplitude required for the material to last 250 million cycles [10].

By using the critical strain range as an criteria for judging fatigue failure, it becomes clear where the first wall is likely to fail. A plot of alternating strain range versus distance through the wall shows that strain will exceed the critical value in the first 60 μm of the wall (Fig. 11). Further in from the surface, the strain range drops below the critical strain range, indicating safe operation. This indicates that for the service life of a first wall, only the front surface will fail from fatigue, while the bulk of the wall should remain intact. The fatigue on this front surface will take the form of small cracks, propagating into the wall.

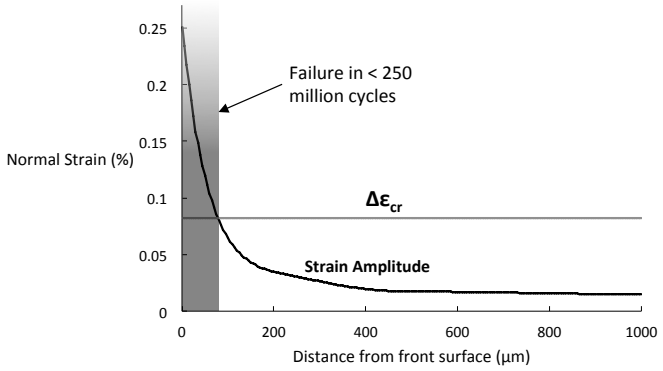

Figure 11: In the 60 μm closest to the surface, strain amplitude exceeds the critical fatigue range necessary for 250 million cycles.

3.3. Crack arrest prediction using J-integral

Exceeding fatigue limits in a small percentage of the bulk volume of the first wall is not necessarily catastrophic. For the fatigue on the surface film to be problematic, there must be enough tensile stress at the crack tips to drive crack propagation towards eventual failure. However, data indicates otherwise; the stress intensity factor actually decreases with increasing crack length for cracks over 25 μm long (see Fig. 12). At this critical length, the stress intensity factor reaches at an absolute maximum of only 3.3 MPa $\sqrt{\text{m}}$, occurring just before every X-ray pulse. While crack propagation rates are not available for HT-9 at this stress intensity range, this value is half of the measured ΔK_{th}, indicating very low or non-existent crack growth.

These stress intensity results were not affected by the stress singularity, as the data were recorded in circumferential element contours ten rows away from the singularity. These contour paths reached a converged solution within two element rows, and reported identical values for every sequential row.

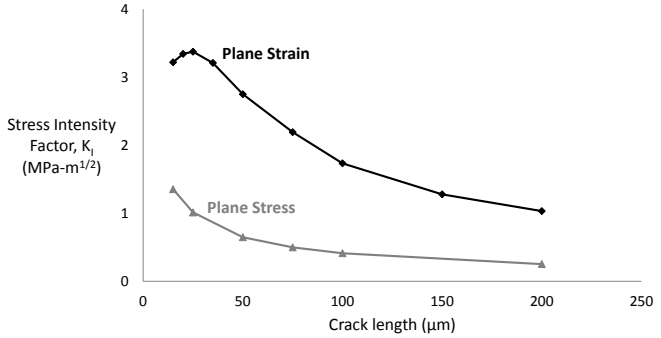

Figure 12: Mode I stress intensity factor decays with increasing crack length due to the decrease in normal tensile stress away from the surface.

After cracks propagate to be 25 μm long, the stress intensity factor decays gradually. This is contrary to common intuition of crack growth, which otherwise might assume a growing crack rate following the equation $K_I = Q\sigma\sqrt{\pi a}$ where a is the crack length, σ is the normal stress, and Q is a geometric modifier. The reason for this behavior, evident in Fig. 9, is due to the spatial variance of tensile stress. During relaxation between X-ray pulses, the tensile stress (which is the driving force for propagation) decreases rapidly away from the fusion-facing surface. As the crack gets longer, the crack tip moves into a region of lower tensile stress, making it less prone to propagate. This influence outweighs the effect of the growing $\sqrt{a}$ term of the linear fracture mechanics equation and results in crack arrest rather than runaway propagation.

Under the analyzed conditions, cracks present on the fusion-facing surface of the steel should not grow significantly into the bulk material. However, this finding disregards effects such as corrosion, temperature, and irradiation, all of which may reduce the material's crack growth threshold. And while though these effects may modify the conclusions, Fig. 12 should still serve as a guide for expected crack propagation under a given crack threshold. For example, if irradiated RAFM steel in a xenon gas at elevated temperature has a threshold crack growth rate of only 2 MPa $\sqrt{\text{m}}$, then cracks should be expected to grow up to almost 100 μm prior to arrest.

4. Conclusions

While the X-ray deposition on the first walls results in plasticity in the first 100 μm, this does not appear to lead to any catastrophic plastic fracture of the wall. The J-integral approach indicates that the stress intensity factors resulting from cyclic thermal loading are insufficient to cause crack growth in HT-9 steel.

This conclusion is based on a broad assumption that the measured material data for HT-9 steel, tested in air at room temperature, will not be categorically different than HT-9 material properties in a fusion environment. Aggressive environments present inside a fusion chamber, such as hydrogen embrittlement and lead and lithium corrosion may significantly affect the material's resistance to cracking, especially over the lifetime of the plant.

Quantifying crack propagation in the presence of fusion-relevant environments will be a critical task for future first wall design. Any experimental campaign in this regard should include accurate simulation of the environment conditions, including irradiation-induced creep and corrosion. Designing the wall temperature to remain below the material's creep threshold may also be important, as creep crack growth could significantly change these conclusions.

Acknowledgments

This work performed under the auspices of the U.S. Department of Energy by Lawrence Livermore National Laboratory under Contract DE-AC52-07NA27344. LLNL-JRNL-610433

HT-9 temperature dependent material properties:

- Conductivity (W/m-K) [11, 12]

$$\begin{aligned} k_{xx} &= 22.927 + 5.342\times10^{-3}T - 1.404\times10^{-7}T^2 \\ &\quad -4.642\times10^{-10}T^3 \end{aligned}$$

- Heat Capacity (J/kg-K) [11]

$$c_p = 289.53 + 0.6T$$

- Density (kg/m^3) [11]

$$\rho = 7874 - 3.23\times10^{-1}T$$

- Thermal Expansion (m/m-K) [11, 12, 13]

$$\begin{aligned} \alpha &= 5.1683\times10^{-6} + 1.5615\times10^{-8}T \\ &\quad -1.1583\times10^{-12}T^2 - 5.143\times10^{-15}T^3 \end{aligned}$$

- Elastic Modulus (MPa) [12]

$$E = 248720 + 92.937T$$

- Modulus of Rigidity (MPa) [11]

$$G = 10.432 \times 10^4 - 53.79T$$

- Poisson's Ratio

$$\nu = 0.1482 + 1.068 \times 10^{-4}T + 1.139 \times 10^{-7}T^2$$

- Plasticity (MPa)
  (EUROFER97 data used as surrogate for HT-9 and simplified to bilinear plasticity) [10]

Temperature	Yield	Tangent Modulus
723	336	2400
773	286	2400
823	242	2400

*Temperature (T) in Kelvin

References

[1] D. Gelles, Effects of irradiation on ferritic alloys and implications for fusion reactor applications, Journal of Nuclear Materials 149 (1987) 192–199.

[2] S. Suresh, Crack initiation in cyclic compression and its applications, Engineering Fracture Mechanics 21 (1985) 453–463.

[3] C. Reid, K. Williams, R. Hermann, Fatigue in compression, Fatigue & Fracture of Engineering Materials & Structures 1 (1979) 267–270.

[4] J. Pope, Rules of thumb for mechanical engineers: a manual of quick, accurate solutions to everyday mechanical engineering problems, Gulf Professional Publishing, 1997.

[5] L. James, Fatigue-crack propagation behavior of ht-9 steel, Journal of Nuclear Materials 149 (1987) 138–142.

[6] F. Huang, Fracture toughness of irradiated ht-9 for structural applications, Nuclear Engineering and Design 90 (1985) 13–23.

[7] Z. Suo, The j integral, `http://imechanica.org/node/7448`, ????

[8] J. Blanchard, C. Martin, Thermomechanical effects in a laser ife first wall, Journal of nuclear materials 347 (2005) 192–206.

[9] N. Dowling, Mechanical behavior of materials: engineering methods for deformation, fracture, and fatigue, prentice Hall Englewood Cliffs, NJ, 1993.

[10] A. Tavassoli, A. Alamo, L. Bedel, L. Forest, J. Gentzbittel, J. Rensman, E. Diegele, R. Lindau, M. Schirra, R. Schmitt, et al., Materials design data for reduced activation martensitic steel type eurofer, Journal of nuclear materials 329 (2004) 257–262.

[11] Alloy Properties Databook, Technical Report 5, Hanford Engineering Development Laboratory, 1981. HEDL-TC-293.

[12] Sandvik HT9 Martensitic Chromium-Molybdenum Steel, Sandvik Steel Catalogue, Technical Report, 1981. S-1,-ENG,.

[13] Nuclear Systems Materials Handbook, Technical Report 2, Hanford Engineering Development Laboratory, Richland, Washington., 1975. TID-26666.